Ni-toughened nc-TiN/a-SiNx nanocomposite thin films

Zhang, Sam; Sun, Deen; Fu, Yongqing; Pei, Y.T.; Hosson, J.Th.M. De

Published in:
Surface & Coatings Technology

DOI:
10.1016/j.surfcoat.2005.08.080

Publication date:
2005

Available online at www.sciencedirect.com

SCIENCE DIRECT

Surface & Coatings Technology 200 (2005) 1530 – 1534

SURFACE & COATINGS TECHNOLOGY

www.elsevier.com/locate/surfcoat

Ni-toughened nc-TiN/a-SiN_x nanocomposite thin films

Sam Zhang [a,*], Deen Sun [a], Yongqing Fu [a], Y.T. Pei [b], J.Th.M. De Hosson [b]

[a] *School of Mechanical and Aerospace Engineering, Nanyang Technological University, 50 Nanyang Avenue, Singapore, 639798, Singapore*
[b] *Department of Applied Physics, Materials Science Center and Netherlands Institute for Metals Research, University of Groningen, Nijenborgh 4, 9747 AG Groningen, The Netherlands*

Available online 16 September 2005

Abstract

Nanocomposite nc-TiN/a-SiN_x thin films containing Ni up to ~40 at.% were prepared by co-sputtering of Ti, TiNi and Si_3N_4 targets in Ar/N_2 gas atmosphere. Adjusting TiNi/(Ti+TiNi) target power ratio altered chemical composition, microstructure and consequently mechanical properties. X-ray photoelectron spectroscopy (XPS), Grazing incidence X-ray diffraction (GIXRD), transmission electron microscopy (TEM) and indentation were used for characterization. With increase of TiNi/(TiNi+Ti) target power ratio from 0 to 1, Ni content increased from 0 to ~40 at.%. XPS results showed that there was no formation of nickel nitride. Nickel existed in a metallic state. GIXRD and TEM results confirmed that the nanocrystalline phase being solid solution of TiN with Si and Ni in its structure, or (Ti, Si, Ni)N. The matrix was amorphous silicon nitride containing metallic nickel. Nanoindentation hardness of the films remained about 30 GPa till Ni addition increases to 4.3 at.%. Toughness was estimated using microindentation method. The K_{IC} increased from 1.15 MPa $m^{1/2}$ without Ni to 2.60 MPa $m^{1/2}$ with 40 at.% Ni while hardness still remained at 14 GPa.

Keywords: Sputtering; Nanostructures; Hardness; Toughness; nc-TiN/a-SiN_x films

1. Introduction

The use of hard coatings in engines, machines, tools and other wear resistant components has achieved a high level of commercial success [1]. Wear resistant, superhard coatings for high speed dry machining would allow the industry to increase the productivity of expensive automated machines and to save on the high costs presently needed for environmentally hazardous coolants [1,2]. Nanocomposite thin films have received much attention recently because they have improved mechanical [3–5] properties owing to the size effect [6,7] and thus are prime candidates for use in dry machining and related applications. Veprek et al. [8] reported that a coating consisting of nc-TiN/a-Si_3N_4/a- and nc-$TiSi_2$ achieved a hardness of 105 GPa via chemical vapor deposition. Zhang et al. [9] prepared nc-TiN/a-SiN_x nanocomposite thin films with hardness about 40 GPa through reactive magnetron sputtering. However, for the majority of applications, achieving the highest hardness is not the primary goal. More important is the appropriate combination of high hardness with toughness, and oxidation resistance, etc.

Irie et al. [10] deposited the TiN–Ni nanocomposite thin films by cathodic arc ion plating. Ni and TiN were selected to contribute toughness and hardness, respectively. In this work, metallic Ni was selected as the toughening phase and nc-TiN/a-SiN_x as the hard phase. Ni-toughened nc-TiN/a-SiN_x nanocomposite thin films were prepared by co-sputtering Ti, TiNi, and Si_3N_4 targets in Ar/N_2 gas atmosphere. The effects of Ni addition on the properties of nc-TiN/a-SiN_x nanocomposite thin films, such as film microstructure, and mechanical properties including hardness and toughness, were systematically studied.

2. Experimental details

2.1. Films preparation

Ni-toughened nc-TiN/a-SiN_x nanocomposite thin films were prepared through co-sputtering of Ti (99.99%), TiNi

* Corresponding author. Tel.: +65 6790 4400; fax: +65 6791 1859.
E-mail address: msyzhang@ntu.edu.sg (S. Zhang).

0257-8972/$ - see front matter © 2005 Elsevier B.V. All rights reserved.
doi:10.1016/j.surfcoat.2005.08.080

(atomic ratio of 50/50, 99.99%) and Si_3N_4 (99.999%) targets in an Ar/N_2 atmosphere using magnetron sputtering system. Silicon (100) wafers with a diameter of 10.16 cm and thickness of 450 μm were used as substrates. The substrates were ultrasonically cleaned in acetone before deposition. The substrate holder was rotated at 15 rpm during the deposition for uniformity. The deposition chamber was pumped to a base pressure of 1.33×10^{-5} Pa, and during deposition the gas pressure was maintained at 0.67 Pa. The flow rate of both Ar and N_2 gases was 15 sccm. The substrate was placed at a distance of 100 mm from the sputtering targets. The depositions were performed at a substrate temperature of 450 °C. In this study, eight types of Ni-toughened nc-TiN/a-SiN_x nanocomposite thin films were prepared through changing target power densities of TiNi, Ti and Si_3N_4. Details of the deposition parameters were tabulated in Table 1.

2.2. Film characterization

The thickness of the films was determined to be around 700 nm by cross-sectional scanning electron microscopy (SEM, JEOL JSM-5600LV). Film composition was obtained by X-ray photoelectron spectroscopy (XPS) analysis using a Kratos-Axis spectrometer with monochromatic Al K_α (1486.71 eV) X-ray radiation (15 kV and 10 mA) and hemispherical electron energy analyzer. The survey spectra in the range of 0–1100 eV were recorded in 1 eV step for each sample, followed by high-resolution spectra over different element peaks in 0.1 eV step, from which the detailed composition was calculated. Curve fitting was performed after a Shirley background [11] subtraction by non-linear least square fitting using a mixed Gaussian/Lorentzian function. To remove the surface contamination layer, Ar ion bombardment was carried out for 15 min using a differential pumping ion gun (Kratos MacroBeam) with an accelerating voltage of 4 keV. The bombardment was performed at an angle of incidence of 45° with respect to the surface normal. The spectra were referenced to the C 1s line of 284.6 eV [12] after ion beam sputtering of surface layer. The chemical compositions of the as-prepared nanocomposite thin films were also entered in Table 1.

For TEM studies, the nanocomposite films with a thickness of about 50 nm were deposited on potassium bromide (KBr) pellets, and then the coated pellets were gently put in distilled water to float off the films. The obtained films prepared by this exfoliation method were examined using a JEOL JEM 2010 TEM with acceleration potential of 200 kV. The experimental and analysis details can be found in Ref. [9]. The microscopy investigation of the detailed nanostructures of the films was carried out with a high-resolution TEM (HR-TEM) (JEOL 4000 EX/II, operated at 400 kV).

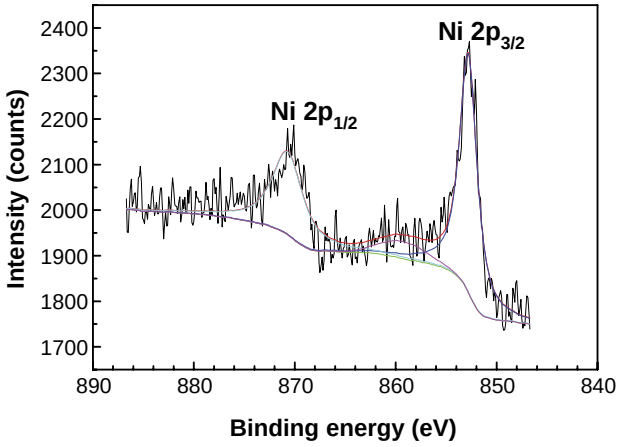

Fig. 1. Ni 2p core level spectrum.

Film crystallinity was also characterized using grazing incidence X-ray diffraction (GIXRD). A Rigaku X-ray Diffractometer MAX 2000 with Cu K_a radiation ($\lambda = 0.15418$ nm) at a scan rate of 2°/min was employed to test the thin films. The scanning was performed from 25° to 90° at a step size of 0.032° and incident angle 1.5°. The lattice parameter of the nanocrystalline TiN was calculated according to peak positions or the distance between the crystal planes [13].

Film hardness was evaluated using a Nano II™ nanoindenter with a Berkovich indenter tip. The indentation depth was chosen as 50 nm that was less than one tenth of the film thickness to avoid possible influence from the substrate. At least five indentations were made on each sample. The results were an average of these readings analyzed by Oliver–Pharr method [14]. The standard deviation of the readings was plotted as the error.

Film toughness was evaluated using indentation method with Micro hardness tester (DMH-1) with a Vickers

Table 1
Sputtering conditions and film characteristics

Sample code		P1	P2	P3	P4	P5	P6	P7	P8
Power density and ratio	Si_3N_4 (W/cm^2)	6.6	6.6	6.6	6.6	6.6	6.6	6.6	4.4
	TiNi (W/cm^2)	0.0	0.2	0.7	1.1	1.4	1.6	2.2	4.4
	TiNi/(TiNi+Ti)	0.00	0.04	0.12	0.20	0.25	0.30	0.40	1.00
XPS chemical composition (at.%)	Ni	0	2.1	4.3	6.3	13.0	16.4	19.0	38.8
	Ti	35.7	37.2	33.2	29.3	26.2	26.6	27.4	26.8
	Si	12.5	10.6	14.0	15.3	17.0	14.1	11.5	4.7
	N	51.8	50.1	48.5	49.1	43.8	42.9	42.1	29.7

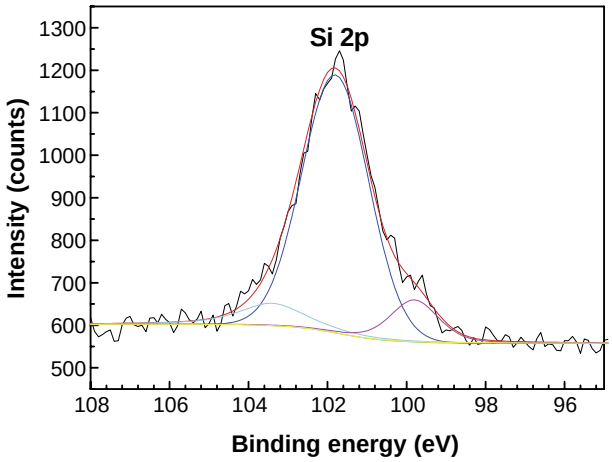

Fig. 2. Si 2p core level spectrum.

indenter. Indentation was conducted at loads of 1000, 500, 300, 200, 100, 50 and 25 g. For each load, at least three readings were obtained. The toughness K_{IC} was obtained through [15]:

$$K_{IC} = \delta\left(\frac{E}{H}\right)^{1/2}\left(\frac{P}{c^{3/2}}\right) \quad (1)$$

where c is the crack length, P the indentation load, E and H are the film elastic modulus and hardness, respectively. δ is an empirical constant which depends on the geometry of the indenter, with 0.016 for the Vickers indenter in use. In order to deduce the film toughness from the substrate affected data, K_{IC} values obtained from Eq. (1) are plotted and then the curve is extrapolated to the depth of about one-tenth of the film thickness to obtain the film toughness.

3. Results and discussions

3.1. XPS core level spectrum of Ni and Si

Fig. 1 shows the Ni 2p core level spectrum. The peaks at the binding energy value of 852.8 and 870.7 eV are confirmed as $2p_{3/2}$ and $2p_{1/2}$ of metallic nickel, respectively. The peak at 859.3 eV is a satellite peak probably due to the consequence of sputtering-damaged crystallites [16]. Nickel nitride has not been detected, as nickel would not react with N_2 because formation of nickel nitride is thermodynamically less favorable than that of TiN [10,17]. Fig. 2 shows the Si 2p core level spectrum. Three chemically distinct components are found in the Si 2p core level photoelectron spectrum. The peak at 101.8 eV is attributed to Si–N bonds of stoichiometric Si_3N_4. Another weak component at about 103.4 eV corresponds to Si–O bonds. Traces of Si peak (at 99.6 eV) can be detected, belonging to free silicon. As we reported in Ref. [18], there is no TiSi detected. A detailed XPS studies of the amorphous phase shows that the amorphous matrix has 80.1 at.% Si–N bonding, 9.1 at.% Si–O bonding and free silicon Si–Si bonding 10.8 at.%. Although most of the Si atoms are believed involved in Si–N bonds of stoichiometric Si_3N_4, there are non-negligible Si–O and Si–Si bondings. To acknowledge this deflection in stoichiometry, we designate the amorphous matrix as a-SiN_x instead of a-Si_3N_4.

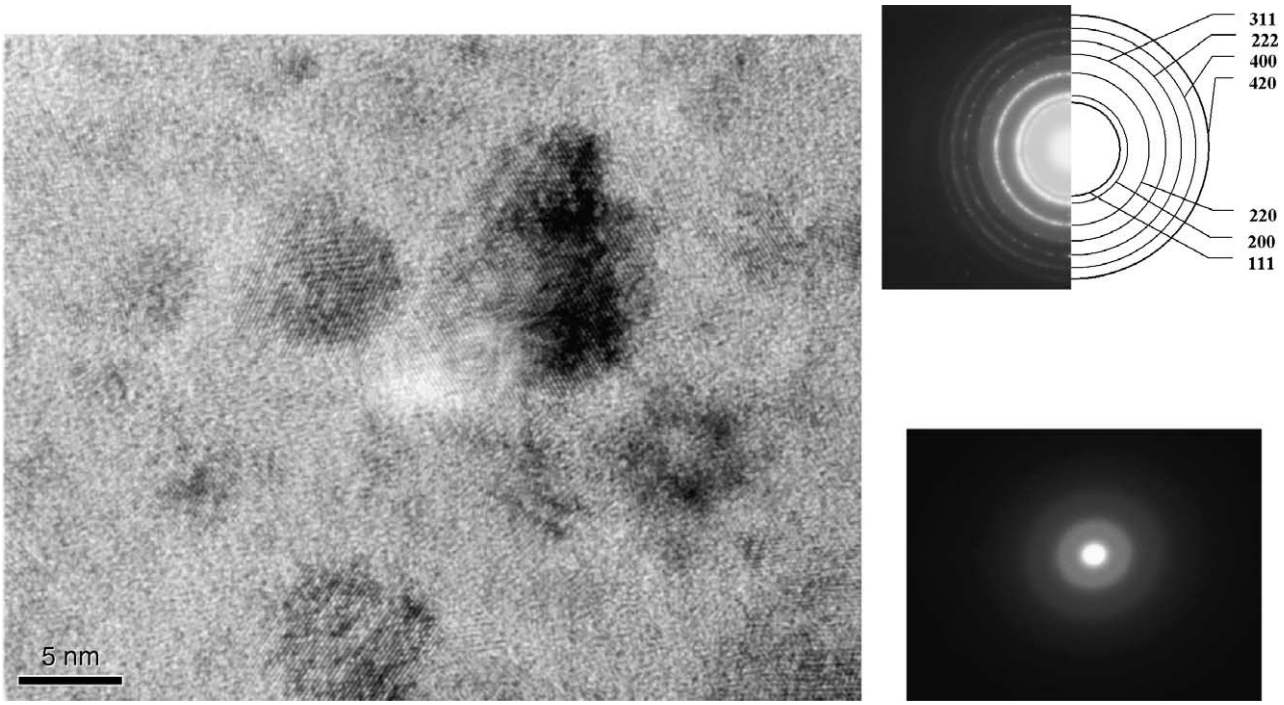

Fig. 3. TEM bright field micrograph of Ni-toughened nc-TiN/a-SiN_x nanocomposite thin film with 2.1 at.% Ni (Sample P2), including SAD patterns of the crystallite phase and amorphous matrix.

3.2. Microstructure

3.2.1. Crystalline and amorphous matrix

An HR-TEM image is shown in Fig. 3 to reveal the nanostructure of Ni-toughened nc-TiN/a-SiN_x nanocomposite thin film with 2.1 at.% Ni (sample P2). Nano-sized crystallites are homogeneously embedded in the amorphous matrix. Analysis of the SAD patterns shows that these crystallites are nano-crystalline TiN. No crystalline Ni, TiSi and Si_3N_4 are found. In general, (111), (200) and (220) TiN crystallographic planes exhibit more distinct rings than other diffraction rings. Proof of the crystallites being TiN and of nano-size also comes from the analysis of the GIXRD pattern (cf. Fig. 4). Ignoring microstrain effect, application of Scherrer's formula estimates the size of the TiN crystallites being: 8.8 nm (2.1 at.% Ni), 7.8 nm (6.3 at.% Ni) and 4.4 nm (16.4 at.% Ni), in good agreement with the HR-TEM observation. In addition, no peaks from crystalline metallic Ni and Si_3N_4 can be identified in the GIXRD patterns. SAD analysis of the matrix demonstrates a diffused pattern typical of an amorphous phase (cf. Fig. 3). Together with the XPS analysis, where nickel is in the metallic state and silicon is in Si–N bond, the results suggest that the matrix is amorphous silicon nitride with amorphous metallic Ni or a-SiN_x(Ni).

3.2.2. Lattice parameter

Fig. 5 plots the lattice parameter of the nc-TiN crystallites calculated using the GIXRD patterns. Without doping of Ni (sample P1), the lattice parameter of nc-TiN is 0.41889 nm. However, pure TiN crystals should have a lattice constant of 0.42417 nm (JCPDS 38-1420). This is because the nc-TiN embedded in a-SiN_x already forms a solid solution with Si to become nc-(Ti,Si)N. Since Si^{4+} has a radius of 0.041 nm, only about half of that of Ti $^{3+}$(0.075 nm) [19], substitution of Ti with Si results in a reduction in the lattice parameter [20]. With increasing the power ratio of TiNi/(TiNi+Ti) targets from 0 to 0.3, the lattice parameter decreases from

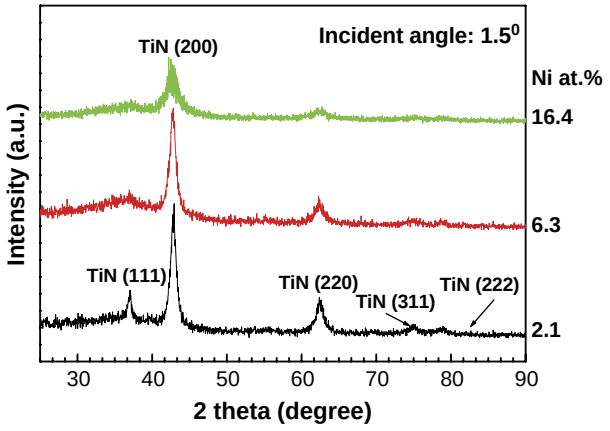

Fig. 4. GIXRD patterns of Ni-toughened nc-TiN/a-SiN_x nanocomposite thin films with 2.1 at.% Ni (Sample P2), 6.3 at.% Ni (Sample P4), and 16.4 at.% Ni (Sample P6).

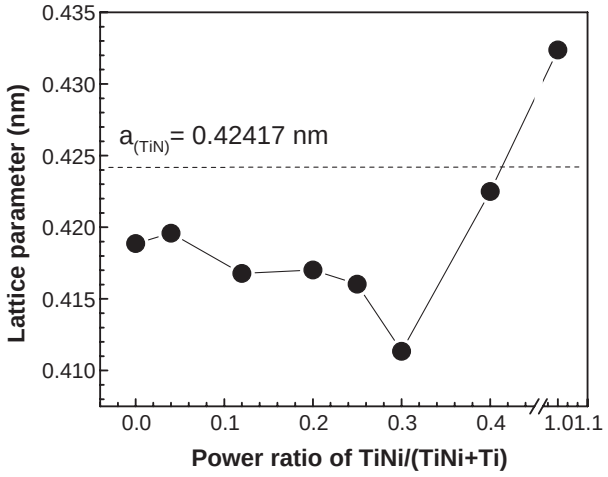

Fig. 5. Calculated lattice parameter nc-TiN as a function of target power ratio of TiNi/(TiNi+Ti).

0.41889 to 0.41135 nm. With further increasing the power ratio to unity, the lattice parameter increases to 0.43237 nm. Since the ionic radius of Ni^{3+} (0.056 nm [21]) is less than that of Ti^{3+} (0.075 nm), the reason for a smaller lattice parameter of (Ti,Si)N at the power ratio $\leq$0.3 is clear: Ni enters nanocrystalline (Ti,Si)N by substituting Ti, thus forming nc-(Ti,Si,Ni)N. When the target power ratio of TiNi/(TiNi+Ti) becomes greater than 0.3, nc-(Ti,Si,Ni)N becomes saturated with Ni; thus a further increase in Ni forces it to enter in the interstitial position. This results in an abrupt increase in lattice parameter.

3.3. Mechanical properties

3.3.1. Hardness

Fig. 6 displays the relationship between the hardness and the Ni content of the nc-TiN/a-SiN_x nanocomposite thin films, including a typical nanoindentation load–depth profile. The measured hardness increases from 28 to 33

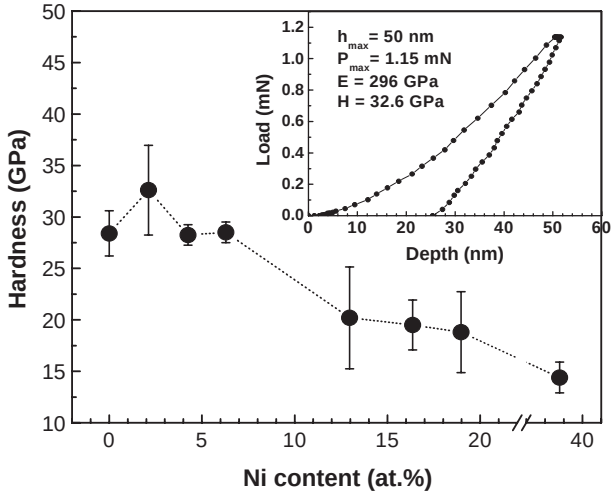

Fig. 6. Hardness varying with Ni content in the Ni-toughened nc-TiN/a-SiN_x nanocomposite thin films.

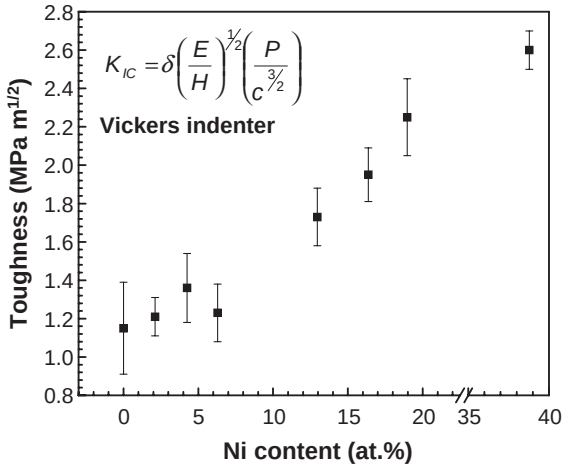

Fig. 7. Toughness as a function of Ni content.

GPa as Ni content increases from 0 to about 2.1 at.%, probably due to slight lattice distortion. A further increase in Ni brings about a decrease in hardness from 33 GPa at 2.1 at.% Ni to 14 GPa at 38.8 at.% Ni. As a general trend, increasing of Ni reduces the crystallite size of TiN (cf. Section 3.2), which effectively increases the separation between the crystallites. In this case, the main contribution of the hardness comes from the matrix. Increase of a soft metallic Ni phase in the matrix naturally reduces its hardness.

3.3.2. Toughness

Fig. 7 shows the toughness of the Ni-toughened nc-TiN/a-SiN_x nanocomposite thin films as a function of Ni content. Compared with the high hardness of the nc-TiN/a-SiN_x nanocomposite thin film (Sample P1) where there is no Ni, the Ni-toughened nc-TiN/a-SiN_x nanocomposite thin films (Sample P2 to P8) exhibit a continuously increased toughness with Ni-content. However, the increase in toughness is much slower for films with lower Ni content ($<\sim 6.3$ at.% Ni) compared with those with higher Ni content. Within the low Ni region, the toughness increase is probably due to the increase of compressive stress induced by ion bombardment. Since cracking is generally initiated by tensile stresses, compressive residual stress in thin films has to be overcome first; thus, the coated component takes more tensile strain (thus the toughness is increased [22]). In the high Ni region, though ion bombardment-induced compressive stress also exists, possible mechanisms for toughness enhancement are as follows: The amorphous state can be described as a state in which density fluctuations exist. These give rise to a distribution of local stresses, hydrostatic as well as shear components. In particular the shear components respond to the applied loading. Ni clusters are able to reduce these stress fields. As a consequence localization of shear bands that lead to low toughness is hampered. It leads to delocalization of crack propagation and further suppression of crack nucleation in the amorphous matrix [23]. The ductility and therefore the toughness of a nanocomposite film will be enhanced provided the particle size d becomes of the same size as the width of the shear bands (or in another word, the separation width of particles) s, i.e. $s \approx d$.

4. Conclusions

Co-sputtering of Ti, TiNi and Si_3N_4 targets produced nanocomposite films where nanocrystals are imbedded homogeneously in the amorphous matrix. The amorphous matrix is mainly Si_3N_4 doped with metallic Ni or a-SiN_x(Ni). The nanocrystalline phase is nc-(Ti,Si,Ni)N. Doping from 0 to $\sim$40 at.% Ni brings about an increase in toughness from 1.15 to 2.60 MPa m$^{1/2}$ at some expense of hardness (from 30 to 14 GPa).

References

[1] T. Cselle, A. Barimani, Surf. Coat. Technol. 76–77 (1995) 712.
[2] Stan Veprek, J. Vac. Sci. Technol., A 17 (5) (1999) 2401.
[3] S. Veprek, S. Reiprich, Thin Solid Films 268 (1995) 64.
[4] S. Zhang, D. Sun, Y. Fu, H. Du, Surf. Coat. Technol. 167 (2003) 113.
[5] S. Zhang, D. Sun, Y. Fu, J. Mater. Sci. Technol. 18 (6) (2002) 485.
[6] B. Cantor, C.M. Allen, Scr. Mater. 44 (2001) 2055.
[7] A.I. Gusev, Physics Uspekhi 41 (1) (1989) 49.
[8] S. Veprek, A. Niederhofer, K. Moto, Surf. Coat. Technol. 133–134 (2000) 152.
[9] S. Zhang, D. Sun, Y. Fu, H. Du, Thin Solid Films 447–448 (2004) 462.
[10] M. Irie, H. Ohara, A. Nakayama, N. Kitagawa, T. Nomura, Nucl. Instrum. Methods Phys. Res., B 121 (1997) 133.
[11] D.A. Shirley, Phys. Rev., B 5 (12) (1972) 4709.
[12] T.L. Barr, S. Seal, J. Vac. Sci. Technol., A 13 (3) (1995) 1239.
[13] S. Zhang, C.D. Qin, L.C. Lim, Int. J. Refract. Met. Hard Mater. 12 (1994) 329.
[14] W.C. Oliver, G.M. Pharr, J. Mater. Res. 7 (1992) 1564.
[15] B.R. Lawn, A.G. Evans, D.B. Marshall, J. Am. Ceram. Soc. 63 (1980) 574.
[16] Y. Fu, H. Du, S. Zhang, Thin Solid Films 444 (2003) 85.
[17] M.F. Zhu, I. Suni, M.-A. Nicolet, J. Appl. Phys. 56 (10) (1984) 2740.
[18] S. Zhang, D. Sun, Y. Fu, H. Du, Q. Zhang, Diamond Relat. Mater 13 (2004) 1777.
[19] B.H. Park, Y. Kim, K.H. Kim, Thin Solid Films 348 (1999) 210.
[20] F. Vaz, L. Rebouta, B. Almeida, P. Goudeau, J. Pacaud, J.P. Riviere, J.B. Sousa, Surf. Coat. Technol. 120–121 (1999) 166.
[21] A. Mehta, P.J. Heaney, Phys. Rev., B 49 (1) (1994) 563.
[22] S. Hogmark, S. Jacobson, M. Larsson, Wear 246 (2000) 20.
[23] Y.T. Pei, D. Galvan, J.Th.M. De Hosson, Nanostructure and properties of TiC/a-C:H composite coatings, Acta Mater., (in press).